High Temperature Annealing of Ion Irradiated Tungsten

Francesco Ferroni[a], Xiaoou Yi[a,d,1], Kazuto Arakawa[b,c], Steven P. Fitzgerald[a], Philip D. Edmondson[e], Steve G. Roberts[a,d]

[a] *Department of Materials, University of Oxford, Parks Road, Oxford, OX1 3PH, UK*
[b] *Department of Materials Science, Faculty of Science and Engineering, Shimane University, 1060 Nishikawatsu, Matsue 690-8504, Japan*
[c] *CREST, JST, 7, Gobancho, Chiyoda-ku, Tokyo 102-0076, Japan*
[d] *EURATOM/CCFE Fusion Association, Culham Science Centre, Abingdon, Oxfordshire OX14 3DB, UK*
[e] *Materials Science and Technology Division, Oak Ridge National Laboratory, Oak Ridge, TN 37831, USA*

Abstract

Transmission electron microscopy of high temperature annealing of pure tungsten irradiated by self-ions was conducted to elucidate microstructural and defect evolution in temperature ranges relevant to fusion reactor applications (500-1200°C). Bulk isochronal and isothermal annealing of ion irradiated pure tungsten (2MeV W^+ ions, 500°C, $10^{14}W^+/cm^2$) with temperatures of 800, 950, 1100 and 1400°C, from 0.5 to 8 hours, was followed by *ex situ* characterisation of defect size, number density, Burgers vector and nature. Loops with diameters larger than 2-3 nm were considered for detailed analysis, among which all loops had $\boldsymbol{b} = {}^1/_2\langle 111\rangle$ and were predominantly of interstitial nature. *In situ* annealing experiments from 300 up to 1200°C were also carried out, including dynamic temperature ramp-ups. These confirmed an acceleration of loop loss above 900°C. At different temperatures within this range, dislocations exhibited behaviour such as initial isolated loop hopping followed by large-scale rearrangements into loop chains, coalescence and finally line-loop interactions and widespread absorption by free-surfaces at increasing temperatures. An activation energy for the annealing of dislocation length was derived, finding

[1] Correspondence author: Xiaoou Yi, xiaoou.yi@materials.ox.ac.uk. Full text available on Acta Materialia, doi:10.1016/j.actamat.2015.01.067

$E_a = 1.34 \pm 0.2$eV for the 700-1100°C range.

1. Introduction

Tungsten is seen as the primary candidate material for plasma-facing components (PFCs) in future fusion reactors. Pure tungsten has been chosen as ITER's PFC material [1], and substantial research is being undertaken internationally to improve its performance (through alloying, tailoring microstructure [2], and compositing), and to understand its fundamental mechanical behaviour [3]. A major issue with tungsten is its acute brittleness and high brittle-to-ductile transition temperature (BDTT) of $\sim$400$-$500°C [4, 5, 6], rendered more severe by radiation damage, which immediately creates dislocation loops and other defect structures (SIAs, voids), and in the longer term can produce brittle phases as a result of elemental transmutation, both of which are detrimental to tungsten's mechanical performance [7].

This paper attempts to address questions arising when tungsten is irradiated in high temperature environments found in fusion reactors. What is the behaviour of radiation damage at high temperatures in tungsten? What evolution pathway do loops found in typical irradiated samples undertake, and can dislocations be annealed away completely, and at what temperature? To this aim, in order to understand the recovery behaviour of displacement damage, transmission electron microscopy (TEM) analysis, used successfully on other materials [8, 9], was performed on ultra-high purity (UHP) tungsten samples following 2MeV W^+ ion irradiation (as a surrogate for neutron irradiation) and subsequent vacuum annealing. The annealing temperatures ranged from 800°C to 1400°C, for times ranging from 1 to 8 hours.

Finally, *in situ* annealing experiments were carried out, both isochronal tests and dynamic ramp-up tests, detailed in subsequent sections. These were useful to observe dislocation behaviour during annealing and to understand the underlying mechanisms associated with damage evolution, as well as the transition between recovery stages and the role which free surfaces play.

1.1. Previous recovery studies

Several studies have probed the effect of temperature *during* irradiation in tungsten, using ion irradiation [10] and neutrons [11]. Numerous studies have also been undertaken with regard to the recovery of irradiation-induced defects post-irradiation. However, these have mostly centred around resistivity measurements [12, 13, 14, 15, 16, 17, 18, 19], with some early field ion microscopy work [20, 21] and a single early TEM study on single crystal tungsten [22]. Similar TEM work has also been done in molybdenum [23]. Resistivity measurements, although useful in identifying the temperature and activation energies of recovery stages (calculated using the Meechan-Brinkman theory [24]), do not provide a direct method of the observation of defects, their nature and how they change with different annealing conditions. This study looks to provide a more complete picture by: 1) quantifying the damage immediately after irradiation, 2) understanding the time and temperature dependence of recovery, 3) directly observing the mechanisms associated with the radiation defect recovery. Such a study has found to be lacking in the literature, with systematic experiments being limited to loops and stacking fault tetrahedra formed during quenching processes of fcc metals [8].

Studies based on fast neutron-irradiated specimens ($\geq$ 1MeV), have identified five stages of annealing common to BCC metals based on the classifications of Thompson [25]. There seem to be numerous inconsistencies in the literature on the number of recovery stages, their nomenclature, temperature and physical interpretation, particularly at higher temperatures [26].

Stage I occurs below -170°C and is attributed to the movement of free interstitials. Stage II, between -170°C and 350°C, is a steady recovery attributed to the release of interstitals from traps with a wide range of interaction energies from 0.25$-$1.7eV [27]. This explains the many sub-stages observed for example in resistivity studies [17]. These two stages occur below fusion reactor operating temperatures, and will not be considered further here. For fusion-relevant temperatures (from 500-1000°C [28]), the recovery of defects created by fast neutrons in tungsten has been observed to occur in three major stages (III-V),

at $\sim 0.15T_m/350°C$, $\sim 0.22T_m/640°C$, $\sim 0.31T_m/970°C$ [16].

Stage III, with an onset of ∼350°C and activation energy of ∼1.7eV, was initially considered to be due to self-interstitial migration, primarily to immobile traps [18]. This explanation was later revised to being due to monovacancy mobility activation [29, 30, 31, 27]; this interpretation is also supported by DFT calculations [32]. The onset temperature has also been shown to shift to lower temperatures with increasing neutron fluence [13].

Higher temperature recovery stages in tungsten have been largely un-researched since the 1970s, with interpretation being limited to resistivity measurements and early FIM experiments [17, 33, 20].

Stage IV recovery, at $0.22T_m$, is still subject to debate [14], being generally attributed to vacancy-impurity complexes [33], or di-vancancies [17]. Recent DFT simulations have shown that di-vancancies are not favoured in tungsten [34]. Other *ab initio* computational studies yield activation energies between 3.00-3.43eV for vacancy-carbon complexes, that may explain this stage as being controlled by the dissolution of vacancy-carbon complexes [35], noting that the experimental activation energy calculated from resistivity measurements is 3.3eV [15]. Similar conclusions for this stage may be drawn by comparing to other materials, such as α-Fe, where the recovery stage above Stage III observed by simulations and positron lifetime measurements was ascribed to VC_n complexes [36, 37, 38].

Stage V recovery, starting at $0.31T_m$ [2], was initially explained as being due to vacancy migration, based on early field-ion microscopy studies [20, 21], but later attributed to the disappearance of "defect clusters" or formation of voids [19]. It is still unclear what is the cause of this recovery stage.

The majority of studies have been carried out on polycrystalline tungsten. In single-crystal tungsten [3], defects were found to be stable up to 1900°C, [17] presumably due to the absence of sinks at grain boundaries. Bykov et al [17]

[2] This stage is referred to as Stage IV in [15].

[3] No crystal orientation is given in this study [17].

identified three stages of annealing: 500°C-800°C (Stage IV), 950°C-1200°C (Stage V), and 1200°C-1900°C (Stage VI).

1.2. Irradiation-induced defects

Ion irradiation introduces several types of defects in the material such as self-interstitial atoms (SIAs), vacancy clusters, dislocation loops, voids. Damage formation specific to W^+-ion irradiated UHP tungsten (and alloys) has been characterised [39, 40] and shows the presence of both $\frac{1}{2}\langle 111\rangle$ and $\langle 100\rangle$-type Burgers vector loops, as suggested by the Eyre-Bullough mechanism, with a decreasing fraction of the latter with increasing irradiation temperature (from $\sim$79% $\frac{1}{2}\langle 111\rangle$ loop fraction at 300°C to $\sim$90% at 750°C, at 1.5dpa).

2. Experimental Procedure

2.1. Sample Preparation

Polycrystalline ultra-high purity tungsten (typically W >99.996wt%) was sourced from Plansee Gruppe, Austria, in the form of 150μm foils. These contained traces of C (10ppm), P (<10ppm), Si and O (5ppm) impurities. 3mm diameter TEM discs were punched from the foils, and mechanically polished to a thickness of 100μm using diamond lapping films (grit size 15, 9, 6, 3 and 1μm). The discs were then annealed in a vacuum furnace for 24 hours at 1400°C to promote grain growth and to ensure a dislocation-free microstructure. The vacuum furnace used a diffusion pump, and had a pressure below 10^{-6}mbar, to prevent surface contamination. Furthermore, subsequent to annealing, the discs were electropolished in a bath of 0.5wt% NaOH acqueous solution at close to 0°C to remove any potential oxides or contamination during annealing and ensure a mirror-like surface finish.

2.2. Ion Irradiation

The polished bulk samples were irradiated at the National Ion Beam Facility at the University of Surrey, United Kingdom, using W^+ ions at 2MeV, at a temperature of 500°C to a fluence of $1 \cdot 10^{14}$ ions/cm^2, producing an estimated dose of 1.5dpa. The dose rate was $2.73 \cdot 10^{10}$ ions/cm^2/s.

The dose was calculated using SRIM 2008, using a displacement threshold energy of 55.3eV [41]. More details on the SRIM computations can be found in the Appendix.

2.3. Ex situ post-irradiation annealing

After irradiation, samples were annealed isothermally or isochronally (i.e. fixed temperatures for varying times, or at fixed time for varying temperatures), and some kept as control samples. All the annealing conditions are given in Table 1. In order to prevent any contamination of the ion-irradiated surface during the annealing stage, the samples were encapsulated in evacuated quartz tubes (washed thoroughly in acetone and subsequently methanol) at a vacuum pressure of $< 10^{-6}$mbar, and annealed in a muffle furnace with argon atmosphere.

Time (hours)	Temperature (°C)
1, 2, 4, 8	800
0.5, 1, 4	950
1	1100
1	1400

Table 1: Bulk isochronal and isothermal annealing experiments

TEM foils were prepared with a twin-jet electropolisher (TenuPol 5), using a 0.5wt%NaOH acqueous solution close to 0°C. The sample was back-thinned with the irradiated side coated with Lacomit varnish (a type of corrosion resistant coating supplied by Agar Scientific). Once the central part reached electron-transparency (thickness <200 nm), the varnish was removed with a dedicated Lacomit solvent (a mixture of acetone and xylene).

2.4. In situ post-irradiation annealing

For *in situ* annealing experiments, a JEOL2010 TEM with a Gatan 628.TA single-tilt heating holder was used. The vacuum pressure was kept at $\sim 10^{-6}$mbar, and oxide formation was not observed in the analysed regions. *In situ* isochronal anneals of as-irradiated samples were carried out, as well as a dynamic ramp-up experiment. For isochronal anneals, the desired temperature was reached using a $\sim$1400°C/hr ramp rate, to match that of the furnaces used for *ex situ* anneals.

TEM micrographs were taken at room temperature, at the end of the ramp-up, and subsequently every 10 minutes; the dynamics of the damage microstructure was recorded (on mini-DV tapes) throughout the annealing experiment.
In the dynamic ramp-up experiment, the temperature was increased in stages: 100°C every 10 minutes, from 100°C to 1200°C. The temperature ramp rate between temperature levels was ∼3°C/s. This was found sufficiently high to minimise additional annealing between temperatures stages, and low enough to minimise sample drift and deformation. At the end of each 10 minute annealing stage, micrographs were taken.

Time (hours)	Temperature (°C)
2	800
2	950
1	1100

Table 2: *In situ* isochronal annealing experiments

2.5. Dislocation Characterisation Procedure

The transmission electron microscopes used for the *ex situ* analysis were either a JEOL2000FX, or JEOL2100, operating at 200kV and $\sim 10^{-6}$mbar vacuum. Grains were chosen close to the $\langle 001 \rangle$ orientation, as samples following pre-irradiation heat treatment had a predomintantly $\{001\}\langle 110 \rangle$ texture [42]. The same sample area ($\sim 0.25 \mu m^2$) was imaged near three poles, exciting a total of eight independent g-vectors in order to determine the Burgers vectors of loops, using the invisibility criterion for a prismatic dislocation loop [4].The sign of the Burgers vectors and the nature of the loops were extracted from inside-outside contrast (sampling loops >4-5nm in diameter).
It has been shown that foil thickness may considerably change the dislocation structure observed [9]. To ensure consistency throughout the numerous analysed samples, the thickness in analysed regions was maintained constant, and the TEM foil wedge angle was kept low. The local thickness of the samples was

[4]The strict version of the invisibility criterion is $\mathbf{g} \cdot \mathbf{R} = 0$, where $\mathbf{R}$ is the lattice displacement. One can expand it to $\mathbf{g} \cdot \mathbf{b} = 0$ and $(\mathbf{g} \cdot \mathbf{b}) \times \mathbf{u} = 0$, where $\mathbf{u}$ is the dislocation line direction, and $\mathbf{b}$ is the Burgers vector.

estimated by taking the product of the number of thickness fringes observed at the edge of the grain in question, and the extinction distance in tungsten (≈33.2nm for a $\boldsymbol{g}$=(200) condition at 200kV [43]).

For a detailed explanation on how to determine the Burgers vector and nature (interstitial, vacancy) of dislocation loops in TEM, see Refs [44, 45].

3. Bulk Isochronal Annealing Results

3.1. Damage microstructure

Figure 1 provides a qualitative overview of the effect of annealing on the dislocation density in ion-irradiated tungsten: (1) a reduction in loop number density with increasing temperature, (2) an increase in average loop size with increasing temperature (particularly transitioning between 800°C and 950°C), (3) the appearance of line dislocations and networks (presumably as glissile loops collide and coalesce) at 950°C and 1100°C, (4) a complete removal of dislocation structures at 1400°C.

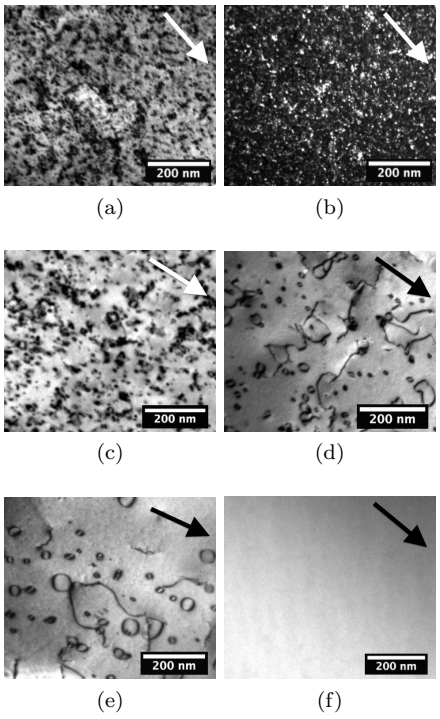

Figure 1: Damage microstructure in (a,b) as-irradiated tungsten (1.5dpa, 2MeV W^+, 500°C) and post-irradiation annealed tungsten subject to conditions of (c) 800°C for 1hr, (d) 950°C for 1hr, (e) 1100°C for 1hr, (f) 1400°C for 1hr. All micrographs shown were imaged close to [001], with $\boldsymbol{g}$=(200) excited. The arrow in each micrograph shows the direction of the g-vector. (b) is weak-beam dark-field ($\boldsymbol{g}$, 3-4$\boldsymbol{g}$), to pick-up the diffraction contrast of very small loops, 1-2 nm, (a) and (c)-(e) are two-beam kinematical bright-field images.

By methodically imaging areas of interest using the procedure detailed above, a complete picture of the loop nature can also be achieved, albeit with increasing uncertainty at lower temperatures (unannealed, 800°C) due to a large number of loops being below <2-3nm in size [44].

3.2. Total loop population

For total loop population, micrographs were recorded in weak-beam dark field conditions of $\boldsymbol{g}$=±(200)/(020), 3-4$\boldsymbol{g}$. Contrast invisibility correction was not deemed necessary, due to lack of observable ⟨100⟩-type dislocation defects, as detailed in later sections.

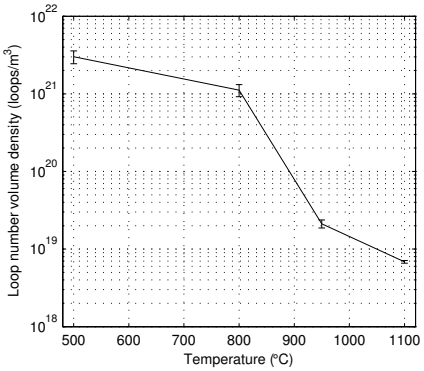

(a)

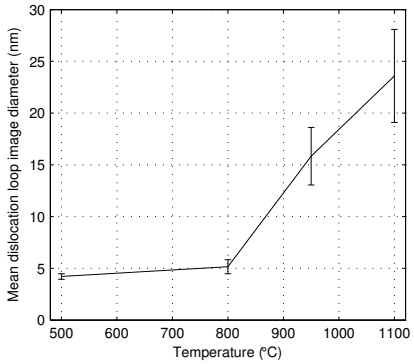

(b)

Figure 2: (a) Variation of loop number density (loops/m^3) with annealing temperature (1hr anneal time), (b) Variation of mean dislocation loop image diameter (nm) with annealing temperature (1hr anneal time). Error bars for the mean loop size are calculated using a 95% confidence interval

.

Figure 2 suggests that there is a transition between 800°C and 950°C, with a two order-of-magnitude reduction in loop number volume density, from $1.1 \cdot 10^{22}$ to $2.1 \cdot 10^{20}$ loops$\cdot$m^{-3}. This is in contrast to the transition between unannealed and 800°C, where loop number density decreases ∼30%, or the transition between 950°C and 1100°C where it is decreased by ∼50%. As temperature is increased, there is greater uncertainty in the *mean* dislocation loop diameter due to the increased scatter (see Figure 4) as well as fewer loops within an imaged area, despite it being easier to accurately measure the size of single dislocation loops.

Nonetheless, it is evident there is an overall increase in size, particularly at 950 and 1100°C.

Dislocation loop size distributions for isochronal anneals are given in Figures 3 and 4, in the form of cumulative and continuous probability distributions respectively. Experimental data in Figure 3 was fitted with a Weibull distribution. This is shown as a continuous probability distribution in Figure 4, overlayed to binned experimental data [5]. To the authors' knowledge, there is no standard fit for the probability density function (pdf) of loop diameters. A Weibull distribution (which was originally proposed for particle size distribution [46]), assumes that there exist processes unknown which generate or annihilate loops of different sizes. With a shape parameter of <1, physical processes are acting to increase the population in the small diameter region, by fragmentation of large loops and/or generation of small ones. Conversely, a shape parameter of >1 indicates that the physical processes are acting to increase the population in the large diameter region, by coalescence of small loops and/or generation of larger ones. Intuitively, as annealing temperature increases, loops collide and merge. This is confirmed by the shape factor k in each temperature pdf being greater than 1 (specifically, $k_{500^\circ C} = 1.9$, $k_{800^\circ C} = 1.4$, $k_{950^\circ C} = 1.3$, $k_{1100^\circ C} = 1.6$). It can be seen that whereas the as-irradiated sample displays dislocation loops with a pronounced peak at ∼3nm diameter, subsequently annealing the sample produces a broader distribution with larger maximum and average loop sizes, increasing with annealing temperature. The loop size distribution broadening is especially evident between the 800°C and 950°C samples. The mean dislocation loop diameter was calculated by measuring their effective area (since the majority are elliptical in shape) and calculating a mean diameter. Sampling in micrographs was done on distinctly visible loops (>1nm). The same procedure was repeated for later isochronal experiments.

[5] The following bin sizes were used: for unannealed and 800°C, binning centers at 1,2,4,6,8,10,13.3,16.6,20,30,50,70,90,100 nanometers were used. For 950°C and 1100°C, binning centers at 0,10,20,30,50,70,90,100 were used. A sample size of 3340 for the unannealed sample, 4940 for 800°C, 1116 for 950°C and 231 for 1100°C was used.

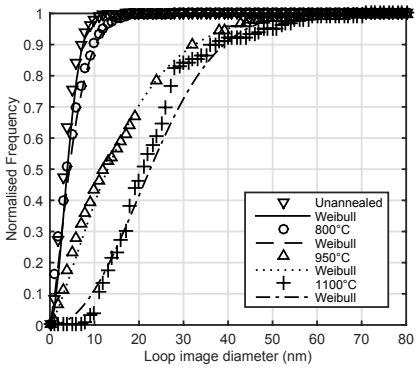

Figure 3: Variation of cumulative probability distribution of dislocation loop image diameter following isochronal annealing (1hr anneal time).

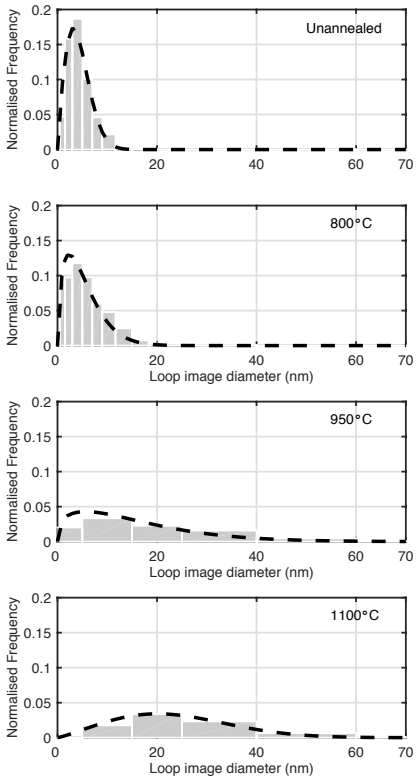

Figure 4: Variation of continuous probability distibution of dislocation loop image diameter following annealing for 1hr shown as dashed lines (using fitted Weibull parameters). Histograms show the binned experimental data.

3.3. Dislocation loop characteristics

Loops having a diameter of >3nm were exclusively of $\mathbf{b}=\frac{1}{2}\langle 111\rangle$-type. For smaller loops, it becomes increasingly difficult to determine **b** reliably. No evidence of $\mathbf{b}=\langle 100\rangle$ vector loops was observed in the annealed samples (50-100 loops analysed per sample, >1nm diameter).

This is consistent with the general trend seen elsewhere [39, 40, 47], of decreasing $\mathbf{b}=\langle 100\rangle$ fractions in UHP-tungsten with increasing irradiation temperature. It is also consistent with the hypothesis that $\langle 100\rangle$ loops are metastable defects which form only in high-energy cascades [47], and that such nano-scale defects can be absorbed in a non Burgers vector-conserving fashion by larger $\frac{1}{2}\langle 111\rangle$ loops [48].

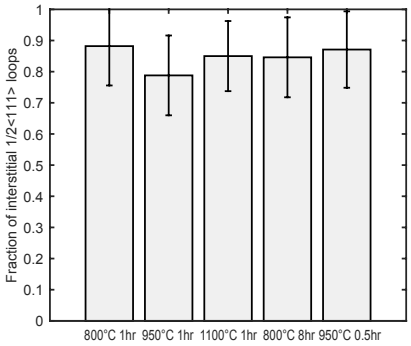

Figure 5: Nature type for dislocation loops analysed in 2MeV 500°C 1.5dpa W^+ irradiated UHP-W, followed by bulk isochronal and isothermal anneals.

Nature analysis was carried out for the isochronal bulk experiments, on an average of 50 loops (>4nm diameter) for each sample. Dislocation loops were found to be predominantly of interstitial type, as shown in Figure 5. The fraction does not appear to vary with annealing treatments, within error (95% confidence interval).

3.4. Voids

The dislocation loops, which were primarily of interstitial type, were clearly visible in the as-irradiated conditions. These defects became significantly mobile

at temperatures above 800°C, and were annealed away completely at 1400°C. On the other hand, the vacancy population produced by self-ion irradiation was unaccounted for, and was presumed to be in the form of vacancy clusters which could not be reliably sized using TEM (<1nm diameter, [44]) in the as-irradiated conditions. Once annealed for 1 hour at 800°C and above, voids became visible in the TEM. Example micrographs (under and over-focus pairs) are shown in Figure 6 and the results are summarised in Figure 7. Until 1100°C the visible voids do not appear to change in size and number density, with an average diameter of ∼1.5±0.1nm, and a density of $\sim 6 \cdot 10^{26}$ voids $\cdot$ m^{-3} . At 1400°C, there is a significant increase in size (∼4.0±0.5nm), and decrease in number density. When performing size measurements for voids, the inside edge of the dark Fresnel fringe in the under-focussed condition was used, as per [44]. The defocus was kept constant at ±1000nm. The measurements were conducted on a JEM 3000F, operating at 300kV.

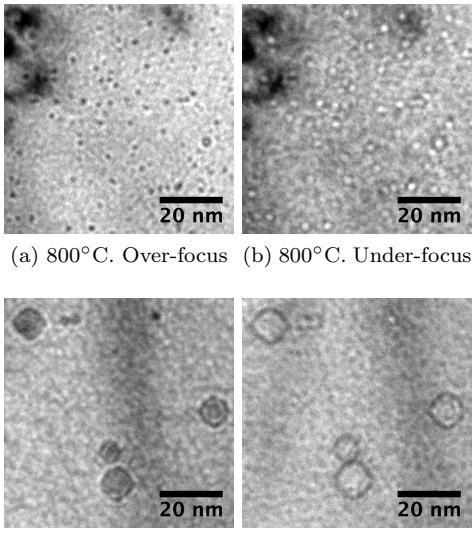

(a) 800°C. Over-focus (b) 800°C. Under-focus

(c) 1400°C. Over-focus (d) 1400°C. Under-focus

Figure 6: Example micrographs of imaged voids at 800°C and 1400°C. The defocus was ±1000nm.

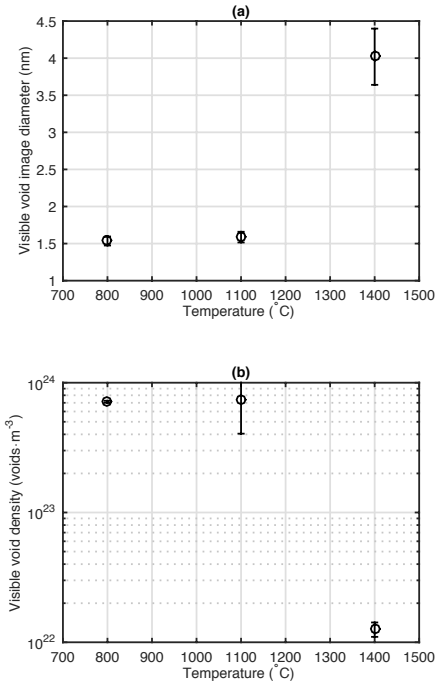

Figure 7: (a) Size (diameter, nm) and (b) number density (voids/m^3) of visible voids in under-focussed condition, for varying temperatures (1hr anneals).

4. Bulk isothermal annealing results

4.1. Total size distribution

It can be seen quantitatively from Figure 8 and qualitatively from Figure 9 that for the temperatures tested, loop growth is not just a temperature-dependent but also time-dependent process. For longer anneals, the loops were larger, at lower densities, and significantly more varied in size. Nonetheless, the rates of loop growth can in principle be compared at different temperatures. For example, a 1hr 950°C anneal yields approximately the same average dislocation loop diameter as a 800°C ∼6.5 hours one. An estimate of activation energies using bulk isothermal annealing data is made in Section 6.2.

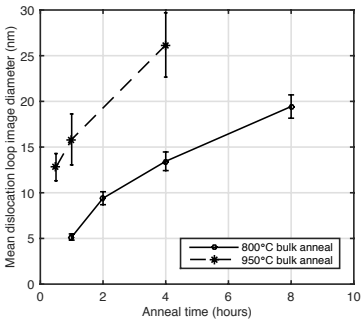

Figure 8: Variation of mean dislocation image diameter (nm) with isothermal bulk annealing (800°C and 950°C annealing temperature).

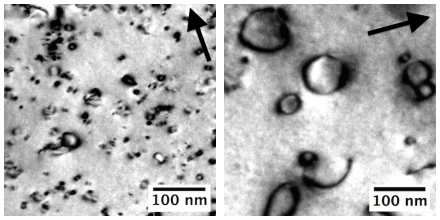

(a) (b)

Figure 9: Damage microstructure after (a) 1hr annealing, (b) 8hr annealing, at 800°C anneal, with ramp-rate of 1400°C/hr. Two-beam kinematical bright-field with $\boldsymbol{g}$=(020) excited.

5. *In situ* annealing results

In situ annealing experiments allow direct observation of the recovery of radiation-induced dislocation loops. Isothermal experiments at 800°C, 950°C and 1100°C were carried out. It was also possible to conduct dynamic temperature ramp-up experiments, results of which are summarised in Figure 10[6].

[6]Video clips of such processes are provided as supplementary material in the online version of the publication

5.1. Dynamic ramp-up

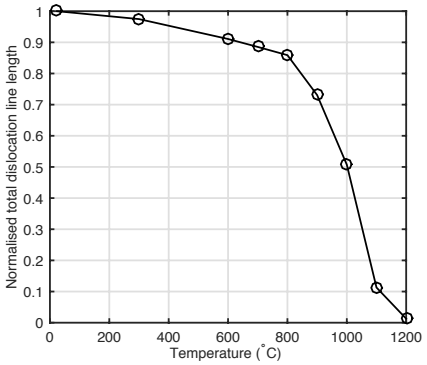

Figure 10: Variation of visible total dislocation line length (normalised to that at room temperature) during ramp-up experiment; the same area was analyzed at each temperature.

From Figure 10, it can be seen that major dislocation line loss begins at ∼900°C (consistent with bulk experiments). At 1100°C, approximately 90% of the dislocation damage has been annealed out. The morphology of the defects has drastically changed, from very small loops with a well-characterised peak of ∼4nm in diameter at as-irradiated temperatures to very large loops (up to ∼70nm diameter) and dislocation lines at 950°C and 1100°C, similarly to the bulk annealed samples (shown in Figure 4).

Figure 11 shows a number of dislocation reactions observed during annealing, mainly loop-loop coalescence, loop annihilation from free surfaces (Figure 12), and loop-line interactions (Figure 13). Intermediate steps for each example are shown with a time label: this signifies the time immediately after the split-second reaction. This is because dislocation motion is generally jerky, whereby a coalescence or interaction event happens within a fraction of a second, followed by periods of relative stability characterised by small vibrations around a stable or pinned configuration. This suggests the events are thermally activated and stochastic in nature, and driven by elastic interactions. The only exception is Figure 11 (a)-(c), in which two loops gradually and steadily move towards a third larger loop in the course of ∼1 minute (a-b), in what appears to be a conservative self-climb process, and subsequently (very quickly) merge (c). A

similar behaviour has been observed in interstitial loops in molybdenum [23], and uranium oxide [49]. This so called self-climb mechanism is explained in [50] as pipe-diffusion of vacancies, although it remains unclear.

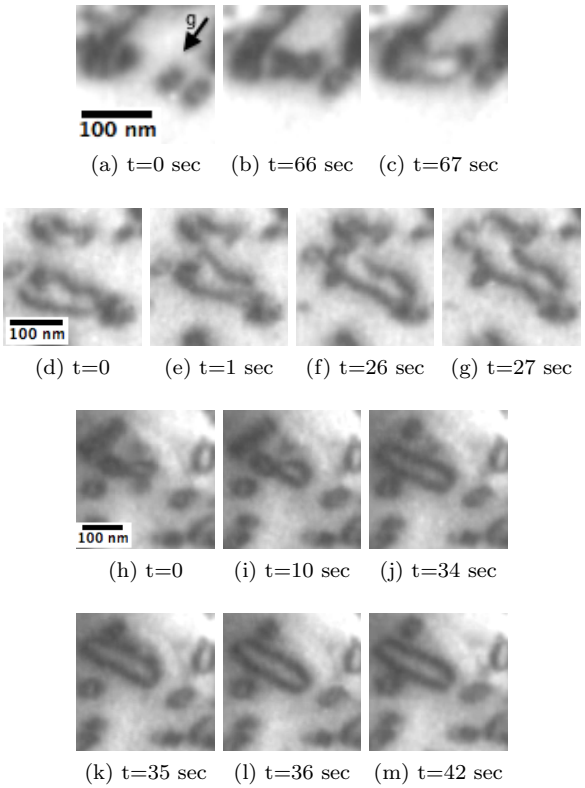

(a) t=0 sec (b) t=66 sec (c) t=67 sec

(d) t=0 (e) t=1 sec (f) t=26 sec (g) t=27 sec

(h) t=0 (i) t=10 sec (j) t=34 sec

(k) t=35 sec (l) t=36 sec (m) t=42 sec

Figure 11: Examples of loop coalescence: (a)-(c) at 900°C, a cluster of loops; (d)-(g) at 1000°C, several loops forming a large irregular loop. (h)-(m) at 1000°C, five loops coalescing into an oblong finger loop. $\boldsymbol{g}=(0\bar{2}0)$ held constant through-out the frames.

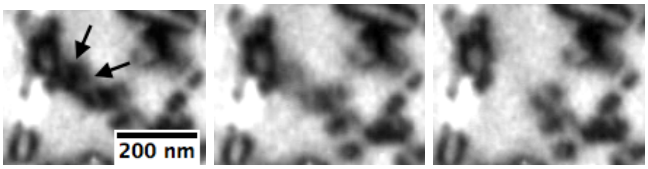

(a) t=0 (b) t=0.05 sec (c) t=0.1 sec

Figure 12: Example of dislocation loops being absorbed by a free surface at 1000°C, as indicated by the pair of arrows in (a). This is a very fast process occurring in a tenth of a second.

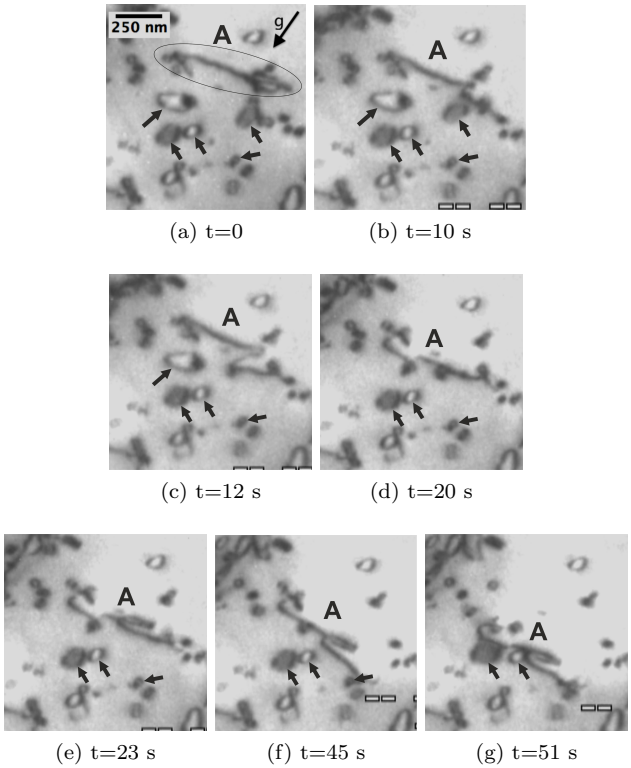

(a) t=0 (b) t=10 s

(c) t=12 s (d) t=20 s

(e) t=23 s (f) t=45 s (g) t=51 s

Figure 13: From *in situ* ramp-up experiment, when held at 1100°C. Example of dislocation line gliding freely, interacting with dislocation loops and either absorbing them or being pinned and released. The dislocation line marked A "sweeps" out other dislocations in its path, marked by arrows

. It develops knots which are subsequently straightened out. Magnification and $\boldsymbol{g}=(0\bar{2}0)$ kept constant for all frames.

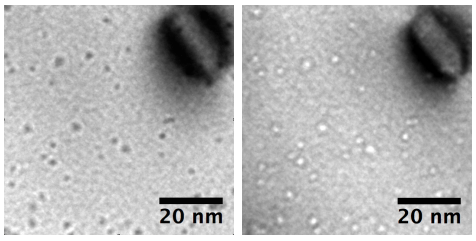

(a) Over-focus (+1000nm) (b) Under-focus (-1000nm)

Figure 14: Appearance of small void-like features after in-situ annealing (T=1200°C) in 2MeV W^+ ion irradiated tungsten.

5.2. Dislocation recovery stages

From closer inspection of the behaviour of dislocation loops at various temperatures during annealing, one can broadly identify the following sequence of events.

1. RT - 300°C: Stable dislocation structure. No loop hopping or loops being absorbed by the surface were observed.
2. 300°C - 700°C: Smaller $\frac{1}{2}\langle 111 \rangle$ loops were seen hopping in 1D, with sporadic loss of loops to the surface, increasing in frequency at higher temperatures.
3. 700°C - 800°C: Reorganisation of loops from a relatively homogenous distribution into discrete "chains" and clusters.
4. 900°C - 1000°C: Coalescence of loops within chains or clusters, examples of which are shown in Figure 11. In the case of chains (where loops rearrange themselves in line, most likely in the same habit plane as this is elastically favourable), coalescence formed oblong finger loops; for clusters (resulting from pinning due to loop-loop interactions), coalescence formed large, sometimes irregularly shaped, dislocation loops. The resulting loops were sometimes observed being subsequently absorbed by the free surfaces (Figure 12), or moving along their glide direction to cluster with another loop. At this temperature, dislocation lines began to be observed.
5. 1000°C - 1200°C: Loss of dislocation loops greatly accelerated, with an additional mechanism: dislocation lines, formed from coalescence and "breaking" of large loops (a surface phenomenon), glided freely in the sample and interacted with dislocation loops in their path. The colliding loops were absorbed into the dislocation line, or occasionally acted as temporary pinning sites for the dislocation line. At higher temperatures, these pinning sites were overcome quickly. Finally, once the dislocation line had finished "sweeping" dislocation lines in its path, it was absorbed by a free surface. This process can be seen in Figure 13. Small void-like features were also observed in the post-annealing characterisation.

6. Discussion

6.1. Defect behaviour

From the bulk isochronal results on number density in Figure 2, there is an accelerated decrease between 800°C and 950°C. From the *in situ* results in Figure 10, one can confirm that loop loss accelerates from 800°C. Despite contradictory information in the available literature on the underlying mechanisms of the recovery stages, several independent experiments on neutron-irradiated pure tungsten recovery, using resistivity as a measure, observed a recovery stage at $\sim$ 970°C. Whereas early work attributed this to migration of single vacancies [15] (largely due to FIM results by [20, 21]), later studies attribute it to defect clustering: "a complex recovery mechanism and could possibly be related to the disappearance of some defect clusters or formation of voids" [19].

From the TEM studies presented here, dislocation loop coarsening and loss occurs at >950°C, suggesting this contributes to the observed 970°C recovery stage found in resistivity experiments. There are some uncertainties involved in directly comparing the two type of experiments. For example, self-ion irradiation produces a relatively shallow region of damage (<200nm for 2MeV W^+) which can be affected by the presence of foil free-surfaces during the annealing experiments, particularly *in situ* ones. This may distort the actual rate of dislocation loss. Nonetheless, it does not change the underlying physical processes activated: there is a clear dependence on temperature. This may be due to the activation of the motion of large dislocation loops and lines decorated with impurities, such as carbon [51], or to vacancy-activated climb leading to coarsening.

Voids can be seen following the bulk 1-hr anneals at $\geq$800°C. However, the mean size and density of the observed voids does not particularly change up to 1100°C. Only in the 1400°C anneal was there a noticeable increase in average size (and decrease in number density). This is consistent with a recovery well above the onset of Stage V recovery, characterised by an enhanced interaction between (now mobile) vacancy clusters.

6.2. Activation energy estimation

The quantity chosen to measure damage recovery was the total dislocation line length per volume, normalised by that measured in the as-irradiated sample. The motivation behind this choice is two fold. Firstly, particularly at higher temperatures, loops turn into lines, making loop area comparisons within the same sample section erroneous. Secondly, radiation damage recovery in the literature has commonly been measured using resistivity. Above the Debye temperature, the electrical resistivity in the kinetic theory approximation is inversely proportional to the electron scattering time. According to Mattheisen's rule, one can write the scattering rate as the sum over possible contributors, such as impurity scattering, electron-phonon scattering and electron-electron scattering. Dislocations (larger ones more so), would have a constant scattering power per *unit length*, as opposed to enclosed area [52, 53]. This is predicated on the idea that the electron-phonon scattering inside a relatively large loop (above ∼1nm diameter) is virtually zero [54].

From Figure 10 (a), we calculate the logarithmic change in normalised dislocation line length between 700°C and 1100°C, and plot it against the inverse of temperature to extrapolate an activation energy from the gradient of the linear fit, as seen in Figure 15. This yields $E_a = 1.34 \pm 0.2$eV.

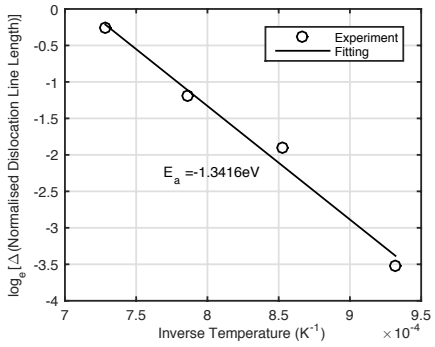

Figure 15: (a) log(y) plot of the change in normalised dislocation line length versus inverse temperature, to extrapolate activation energy.

One can also attempt to estimate an activation energy by looking at the isother-

mal bulk annealing data given in Figure 8. Assuming a linear extrapolation between the 4 and 8 hours data points for 800°C, the mean loop size at ∼6.5hours is equal to a 1-hour anneal. In other words, the loop growth rate at 950°C is ∼6.5 times larger than at 800°C, which yields an activation energy of 1.41±0.1eV.

6.3. Estimation of climb mobility

Equilibrium positions of loops can be found using the isotropic elasticity approximation found in Hirth & Lothe [55]. These elastic interactions have been shown to be the driving force of loop re-organisation into chains via glide [56], with some coalescing due to direct collisions. These chains are clearly visible at ∼800°C in Figure 1.

One hypothesis for increased recovery above 800°C is the activation of dislocation climb. As shown in Figure 11, coalescence seems to occur when two adjacent loops which have reached their elastically-determined equilibrium positions through glide join together via climb, to form oblong loops. For isolated infinite straight dislocations, analytical expressions for climb mobility laws are available [57, 58], which allow estimation of typical timescales expected for climb motion, based solely on vacancies. Assuming a linearly varying dislocation velocity with applied force, climb velocity can be written as (Eq. 1).

$$v_{\mathrm{cl}} = M_{\mathrm{cl}} \left[F_{\mathrm{cl}} + F_{\mathrm{os}} \right] \tag{1}$$

where M_{cl} is the climb mobility, F_{cl} the climb force, and F_{os} the osmotic force. The osmotic force occurs when there is a vacancy supersaturation [58]. However, in the present analysis, it is considered negligible as large loops were not observed growing through processes such as Ostwald ripening. The climb force F_{cl} is the projection of the Peach-Koehler force in the direction perpendicular to the dislocation glide plane and is given by $F_{\mathrm{cl}} = [(\boldsymbol{\sigma b} \times \boldsymbol{\nu}] \cdot \boldsymbol{n}$, where $\boldsymbol{\sigma}$ is the local stress, $\boldsymbol{b}$ the dislocation Burger's vector, and $\boldsymbol{n}$ the climb direction. For two infinitely long straight edge dislocations, the climb force reduces to Eq. 2, where $|\boldsymbol{r}|$ is the separation distance in the climb direction.

$$F_{\mathrm{cl}} = \pm \frac{|\boldsymbol{b}|^2 \mu}{2\pi(1-\nu)|\boldsymbol{r}|} \tag{2}$$

The climb mobility is then given by Eq. 3.

$$M_{\mathrm{cl}}(\theta) = \frac{2\pi D_v \Omega c_0^v}{kTb^2 \sin^2(\theta) ln(r_\infty / r_c)} \tag{3}$$

where Ω the atomic volume, θ the dislocation character [7], k the Boltzmann constant, T the temperature and r_c the inner core radius of the dislocation line. $D_v = D_v^0 \exp\left(\frac{U_v^m}{kT}\right)$, with U_v^m being the vacancy migration energy, D_v^0 the constant prefactor characterising vacancy diffusion, and $c_0^v = \exp\left[-(U_v^f - P\Delta V_v/kT\right]$, where U_v^f is the vacancy formation energy, and ΔV_v the associated relaxation volume. The vacancy migration and formation energies of tungsten, U_v^m and U_v^f, are 1.78 and 3.56eV respectively [59], and the vacancy diffusion prefactor is $\sim 1.5 \cdot 10^{-5}$ m$^2 \cdot$ s^{-1} according to DFT studies [60].

With the above parameters, the climb mobility is extremely low, even for the highest temperatures and smallest segment separations. For example, at 1200°C two segments with 1nm separation would coalesce solely by vacancy-mediated climb in ∼1hr, making this hypothesis very unlikely based on the experimental observations reported here.

7. Conclusion

High temperature isochronal (1hour, 800-1400°C) and isothermal (1-8 hours) annealing of pure tungsten was carried out, followed by post-annealing characterisation. No **b**=⟨100⟩-type loops were found for loops above 2-3nm diameter, only ½⟨111⟩-type, of predominantly interstitial nature. Average loop size increased and loop density decreased with increasing temperature, with a particular acceleration above ∼950°C. Average loop diameter after 1 hour annealing was ∼ 5nm at 800°C (1hr) and ∼ 23nm at 1100°C. Virtually no dislocation defects were observed after annealing at 1400°C for 1 hour.

[7] $\theta = \frac{\pi}{2}$ for pure edge, and 0 for pure screw (capped at a maximum mobility)

In situ annealing experiments up to 1200°C were also carried out, including dynamic temperature ramp-ups. These confirmed an acceleration of loop loss from 800°C. Small dislocation loops were observed hopping from 300°C, increasing in frequency from 500°C. By 800°C, loops had rearranged into loop "chains" or clusters. Increasing the temperature resulted in formation of larger irregular or oblong finger loops from coalescence of smaller loops in such chains. Above 1000°C, dislocation lines moved relatively freely, interacting with smaller dislocation networks and "sweeping" out damage. Small voids ($\sim$ 2nm) were also observed at such high temperatures. The acceleration of loop loss at $\sim$ 1000°C may be related to "Stage V" annealing, as observed in previous resistivity recovery experiments on neutron-irradiated tungsten [26]. Voids were observed in all 1-hr anneals at 800°C, but were found to increase substantially in size (up to $\sim$4nm) and decrease in number density at 1400°C. An activation energy for the annealing of dislocation length was derived from the ramp annealing experiments, finding $E_a = 1.34 \pm 0.2$eV for the 700-1100°C range.

8. Acknowledgements

The authors express their thanks to Dr. Nianhua Peng from the National Ion Beam Centre (United Kingdom), for specimen irradiation. We also extend thanks to Dr. Daniel Mason for helpful discussions. FF was funded by the Engineering and Physical Research Council (EPSRC) Fusion Doctoral Training Centre and EPSRC programme grant "Materials for Fusion and Fission Power" (EP/H018921/1). KA acknowledges the following: Grant-in-Aid for Scientific Research (Grant No. 24360395, 24656371, 24560805, and 22224012) from the Ministry of Education, Sports, Culture, Science and Technology in Japan), and the Iron and Steel Institute of Japan Research Promotion Grant. PDE also acknowledges funding through an EPSRC Career Acceleration Fellowship (EP/K030043/1).

9. Appendix

The damage profile as predicted by SRIM 2008, is given in Figure 16. The simulation was run using the full-cascade mode, using 10,000 implantation events, and extracted from the vacancy.txt files. The peak damage is approximately at ∼100nm depth, quickly falling to relatively negligible levels doses at <300nm. The displacement energy threshold used was 55.3eV [41]. From this, a nominal dose of 1.5dpa was extrapolated.

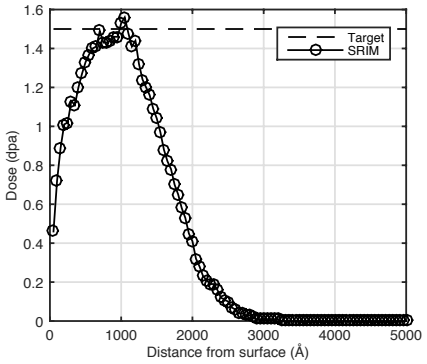

Figure 16: SRIM damage profile, as calculated using SRIM 2008, with a displacement threshold energy of 55.3eV [41].

.

10. References

References

[1] A. Möslang, E. Diegele, M. Klimiankou, R. Lässer, R. Lindau, E. Lucon, E. Materna-Morris, C. Petersen, R. Pippan, J. Rensman, M. Rieth, B. van der Schaaf, H.-C. Schneider, and F. Tavassoli, Towards reduced activation structural materials data for fusion demo reactors, Nuclear Fusion, 45 (7) (2005) 649.

[2] O. El-Atwani, J. a. Hinks, G. Greaves, S. Gonderman, T. Qiu, M. Efe, and J. P. Allain, In-situ TEM observation of the response of ultrafine- and nanocrystalline-grained tungsten to extreme irradiation environments., Scientific Reports, 4 (2014) 4716.

[3] M. Rieth, S. Dudarev, S. G. de Vicente, J. Aktaa, T. Ahlgren, S. Antusch, D. Armstrong, M. Balden, N. Baluc, M.-F. Barthe, W. Basuki, M. Battabyal, C. Becquart, D. Blagoeva, H. Boldyryeva, J. Brinkmann, M. Celino, L. Ciupinski, J. Correia, A. D. Backer, C. Domain, E. Gaganidze, C. García-Rosales, J. Gibson, M. Gilbert, S. Giusepponi, B. Gludovatz, H. Greuner, K. Heinola, T. Höschen, A. Hoffmann, N. Holstein, F. Koch, W. Krauss, H. Li, S. Lindig, J. Linke, C. Linsmeier, P. López-Ruiz, H. Maier, J. Matejicek, T. Mishra, M. Muhammed, A. Muñoz, M. Muzyk, K. Nordlund, D. Nguyen-Manh, J. Opschoor, N. Ordás, T. Palacios, G. Pintsuk, R. Pippan, J. Reiser, J. Riesch, S. Roberts, L. Romaner, M. Rosiński, M. Sanchez, W. Schulmeyer, H. Traxler, A. Ureña, J. van der Laan, L. Veleva, S. Wahlberg, M. Walter, T. Weber, T. Weitkamp, S. Wurster, M. Yar, J. You, and A. Zivelonghi, Recent progress in research on tungsten materials for nuclear fusion applications in europe, Journal of Nuclear Materials, 432 (1–3) (2013) 482 – 500.

[4] A. Giannattasio and S. Roberts, Strain-rate dependence of the brittle-to-ductile transition temperature in tungsten, Philosophical Magazine, 87 (17) (2007) 2589–2598.

[5] A. Giannattasio, Z. Yao, E. Tarleton, and S. Roberts, Brittle-ductile transitions in polycrystalline tungsten, Philosophical Magazine, 90 (30) (2010) 3947–3959.

[6] M. Rieth and A. Hoffmann, Influence of microstructure and notch fabrication on impact bending properties of tungsten materials, International Journal of Refractory Metals and Hard Materials, 28 (2010) 679–686.

[7] D. Armstrong, P. Edmondson, and S. Roberts, Effects of sequential tungsten and helium ion implantation on nano-indentation hardness of tungsten, Applied Physics Letters, 102 (251901) (2013) 1–5.

[8] B. Eyre, Transmission electron microscope studies of point defect clusters

in fcc and bcc metals, Journal of Physics F: Metal Physics, 3 (1973) 422–470.

[9] M. Li, M. Kirk, P. Baldo, D. Xu, and B. Wirth, Study of defect evolution by TEM with in situ ion irradiation and coordinated modeling, Philosophical Magazine, 92 (16) (2012) 2048–2078.

[10] V. Haussermann, A study of the radiation damage produced by energetic gold ions in molybdenum and tungsten, Philosophical Magazine, 25 (1972) 583–598.

[11] T. Tanno, M. Fukuda, S. Nogami, and A. Hasegawa, Microstructural development in neutron irradiated tungsten alloys, Materials Transactions, 52 (7) (2011) 1447–1451.

[12] H. Schultz, D. Erholung, S. Iii, A. Aktivierungsenergie, F. S. Iii, B. Iv, S. V. Fiir, and E. Veriinderung, Die erholung des elektrischen widerstandes kaltverformtem wolfram, Acta Metallurgica, 12 (May) (1964) 649–664.

[13] L. Keys, J. Smith, and J. Moteff, Stage III recovery in neutron irradiated tungsten, Scripta Metallurgica, 1 (1967) 71–72.

[14] L. Keys, J. Smith, and J. Moteff, High-temperature recovery of tungsten after neutron irradiation, Physical Review, 176 (3) (1968) 851–856.

[15] L. Keys, Comparison of the recovery of damage in W and Mo after neutron irradiation, Journal of Applied Physics, 40 (9) (1969) 3866.

[16] L. Keys and J. Moteff, Neutron Irradiation and Defect Recovery of Tungsten, Journal of Nuclear Materials, 34 (1970) 260–280.

[17] V. Bykov, G. Birzhevoi, M. Zakharova, and V. Solov'ev, Nature and Stability of Radiation Defects in Single-Crystal Tungsten, Atomnaya Energiya, 33 (4) (1972) 809–813.

[18] Y.-W. Kim and J. M. Galligan, Radiation Damage and Stage III Defect Annealing in Thermal Neutron Irradiated Tungsten, Acta Metallurgica, 26 (1978) 379–390.

[19] M. S. Anand, B. M. Pande, and R. P. Agarwala, Recovery in neutron irradiated tungsten, Radiation Effects, 39 (3-4) (1978) 149–155.

[20] D. Jeannotte, Energy of motion of vacancies in tungsten, Physical Review Letters, 19 (5) (1967) 232–233.

[21] D. Jeannotte and J. M. Galligan, A study of radiation damage in tungsten - i, Acta Metallurgica, 18 (1970) 71–79.

[22] L. Lacefield, J. Moteff, and J. Smith, Neutron radiation damage in tungsten single crystals, Philosophical Magazine, 13 (125) (1966) 1079–1081.

[23] B. L. Eyre and D. M. Maher, Neutron irradiation damage in molybdenum, Philosophical Magazine, 24 (190) (1971) 767–797.

[24] C. Meechan and J. Brinkman, Electrical Resistivity Study of Lattice Defects Introduced in Copper by 1.25MeV Electron Irradiation at 80K, Physical Review, 103 (5) (1956) 1193–1202.

[25] M. Thompson, The damage and recovery of neutron irradiated tungsten, Philosophical Magazine, 5 (51) (1960) 278–296.

[26] P. Ehrhart, P. Jung, H. Schultz, and H. Ullmaier, Landolt-Bornstein: Atomic Defects in Metals, volume 25, Springer-Verlag, Berlin (1991).

[27] D. Mason, X. Yi, M. Kirk, and S. Dudarev, Elastic trapping of dislocation loops in cascades in ion-irradiated tungsten foils, Journal of Condensed Matter, 26 (37) (2014) 375701.

[28] H. Bolt, V. Barabash, G. Federici, J. Linke, A. Loarte, J. Roth, and K. Sato, Plasma facing and high heat flux materials - needs for iter and beyond, Journal of Nuclear Materials, 307-311 (2002) 43–52.

[29] K.-D. Rasch, R. Siegel, and H. Schultz, Quenching and recovery investigations of vacancies in tungsten, Philosophical Magazine A, 41 (1) (1980) 91–117.

[30] J. N. Mundy, S. T. Ockers, and L. C. Smedskjaer, Vacancy migration enthalpy in tungsten at high temperatures, Philosophical Magazine A, 56 (6) (1987) 851–860.

[31] A. Debelle, M. Barthe, and T. Sauvage, First temperature stage evolution of irradiation-induced defects in tungsten studied by positron annihilation spectroscopy, Journal of Nuclear Materials, 376 (2008) 216–221.

[32] D. Nguyen-Manh, A. Horsfield, and S. Dudarev, Self-interstitial atom defects in bcc transition metals: group-specific trends, Physical Review B, 73 (2) (2006) 020101.

[33] M. Zakharova, V. Solov'ev, and V. Bykov, High-temperature stages of the annealing of radiation defects in refractory bcc metals, Atomnaya Energiya, 38 (2) (1975) 78–81.

[34] L. Ventelon, F. Willaime, C.-C. Fu, M. Heran, and I. Ginoux, Ab initio investigation of radiation defects in tungsten: Structure of self-interstitials and specificity of di-vacancies compared to other bcc transition metals, Journal of Nuclear Materials, 425 (2012) 16–21.

[35] Y. Liu, Z. Dai, and W. Wang, Influence of carbon-vacancy interaction on carbon and vacancy diffusivity in tungsten, Computational Materials Science, 83 (2014) 1–4.

[36] T. Jourdan, C. C. Fu, L. Joly, J. L. Bocquet, M. J. Caturla, and F. Willaime, Direct simulation of resistivity recovery experiments in carbon-doped α-iron, Physica Scripta, T145 (2011) 014049.

[37] D. Terentyev, G. Bonny, A. Bakaev, and D. Van Neck, On the thermal stability of vacancy-carbon complexes in alpha iron., Journal of Physics: Condensed Matter, 24 (38) (2012) 385401.

[38] S. Dudarev, Density Functional Theory Models for Radiation Damage*, Annual Review of Materials Research, 43 (1) (2013) 35–61.

[39] X. Yi, M. L. Jenkins, M. Briceno, S. G. Roberts, Z. Zhou, and M. A. Kirk, In situ study of self-ion irradiation damage in W and W–5Re at 500 °C, Philosophical Magazine, 93 (14) (2012) 1715–1738.

[40] X. Yi, Electron microscopy study of radiation damage in tungsten and alloys, Ph.D. thesis, University of Oxford (Wolfson College) (2013).

[41] F. Maury, P. Vajda, A. Lucasson, and P. Lucasson, Frenkel pair creation and stage i recovery in w crystals irradiated near threshold, Radiation Effects, 38 (1978) 53–55.

[42] D. Armstrong, X. Yi, E. Marquis, and S. Roberts, Hardening of self-ion implanted tungsten and tungsten 5-wt% rhenium, Journal of Nuclear Materials, 432 (2013) 428–436.

[43] P. Hirsch and A. Howie, Electron microscopy of thin crystals, Butterworths (1971).

[44] M. Jenkins and M. Kirk, Characterization of Radiation Damage by Transmission Electron Microscopy, Series in Microscopy in Materials Science Series. Taylor & Francis Group (2001), ISBN 9780750307482.

[45] J. Hinks and S. Donnelly, Copper indium diselenide : crystallography and radiation-induced dislocation loops, Philosophical Magazine, 91 (4) (2011) 517–536.

[46] W. Brown and K. Wohletz, Derivation of the weibull distribution based on physical principles and its connection to the rossin-rammler and lognormal distributions, Journal of Applied Physics, 78 (4) (1995) 2758–2763.

[47] A. Sand, S. Dudarev, and K. Nordlund, High energy collision cascades in tungsten: dislocaiton loops structure and clustering scaling laws, EPL, (103) (2013) 46003.

[48] K. Arakawa, T. Amino, and H. Mori, Direct observation of the coalescence process between nanoscale dislocation loops with different burgers vectors, Acta Materialia, 59 (2011) 141–145.

[49] J. A. Turnbull, The coalescence of dislocation loops by self climb, Philosophical Magazine, 21 (21:169) (1970) 83–94.

[50] J. Narayan and J. Washburn, Self-climb of dislocation loops in magnesium oxide, Philosophical Magazine, 26 (5) (1972) 1179–1190.

[51] K. Arakawa, K. Ono, M. Isshiki, K. Mimura, M. Uchikoshi, and H. Mori, Observation of the one-dimensional diffusion of nanometer-sized dislocation loops, Science, 318 (5852) (2007) 956–9.

[52] Z. S. Basinski, J. S. Dugdale, and a. Howie, The electrical resistivity of dislocations, Philosophical Magazine, 8 (96) (1963) 1989–1997.

[53] R. Brown, Electrical resistivity of dislocations in metals, Journal of Applied Physics: Metal Physics, 7 (7) (1977) 1283–1295.

[54] D. Mason, Private communication (2014), CCFE.

[55] J. Hirth and J. Lothe, Theory of Dislocations, Krieger Publishing Company (1982).

[56] S. Dudarev, K. Arakawa, X. Yi, Z. Yao, M. L. Jenkins, M. Gilbert, and P. Derlet, Spatial ordering of nano-dislocation loops in ion-irradiated materials, Journal of Nuclear Materials, 455 (2014) 16–20.

[57] D. Mordehai, E. Clouet, M. Fivel, and M. Verdier, Introducing dislocation climb by bulk diffusion in discrete dislocation dynamics, Philosophical Magazine, 88 (6) (2008) 899–925.

[58] B. Bakó, E. Clouet, L. M. Dupuy, and M. Blétry, Dislocation dynamics simulations with climb: kinetics of dislocation loop coarsening controlled by bulk diffusion, Philosophical Magazine, 91 (23) (2011) 3173–3191.

[59] P. Derlet, D. Nguyen-Manh, and S. Dudarev, Multiscale modeling of crowdion and vacancy defects in body-centered-cubic transition metals, Physical Review B, 76 (2007) 054107.

[60] L. Bukonte, T. Ahlgren, and K. Heinola, Modelling of monovacancy diffusion in w over a wide temperature range, Journal of Applied Physics, 115 (123504) (2014) 1–5.